

Citation for published version:

Miho N. Ishigaki, Nozomu Tominaga, Chiaki Kobayashi, and Ken'ichi Nomoto, 'FAINT POPULATION III SUPERNOVAE AS THE ORIGIN OF THE MOST IRON-POOR STARS', *The Astrophysical Journal Letters*, Vol. 792 (2), August 2014.

DOI:

<https://doi.org/10.1088/2041-8205/792/2/L32>

Document Version:

This is the Published Version.

Copyright and Reuse:

© 2014 American Astronomical Society.

Content in the UH Research Archive is made available for personal research, educational, and non-commercial purposes only. Unless otherwise stated, all content is protected by copyright, and in the absence of an open license, permissions for further re-use should be sought from the publisher, the author, or other copyright holder.

Enquiries

If you believe this document infringes copyright, please contact the Research & Scholarly Communications Team at rsc@herts.ac.uk

FAINT POPULATION III SUPERNOVAE AS THE ORIGIN OF THE MOST IRON-POOR STARS

MIHO N. ISHIGAKI¹, NOZOMU TOMINAGA^{1,2}, CHIAKI KOBAYASHI^{1,3}, AND KEN'ICHI NOMOTO^{1,4}

¹ Kavli Institute for the Physics and Mathematics of the Universe (WPI), The University of Tokyo, Kashiwa, Chiba 277-8583, Japan; miho.ishigaki@ipmu.jp

² Department of Physics, Faculty of Science and Engineering, Konan University, 8-9-1 Okamoto, Kobe, Hyogo 658-8501, Japan

³ School of Physics, Astronomy and Mathematics, Centre for Astrophysics Research, University of Hertfordshire, College Lane, Hatfield AL10 9AB, UK

Received 2014 April 8; accepted 2014 August 9; published 2014 August 26

ABSTRACT

The most iron-poor stars in the Milky Way provide important observational clues to the astrophysical objects that enriched the primordial gas with heavy elements. Among them, the recently discovered iron-deficient star SMSS J031300.36–670839.3 shows a remarkable chemical composition with a non-detection of iron ($[\text{Fe}/\text{H}] < -7.1$) and large enhancement of carbon and magnesium relative to calcium. We investigate supernova yields of metal-free (Population III) stars to interpret the abundance pattern observed in this star. We report that the high $[\text{C}/\text{Ca}]$ and $[\text{C}/\text{Mg}]$ ratios and upper limits of other elemental abundances are well reproduced with the yields of core-collapse supernovae (which have normal kinetic energies of explosion E of $E_{51} = E/10^{51}$ erg = 1) and hypernovae ($E_{51} \geq 10$) of Population III $25 M_{\odot}$ or $40 M_{\odot}$ stars. The best-fit models assume that the explosions undergo extensive matter mixing and fallback, leaving behind a black hole remnant. In these models, Ca is produced by static/explosive O burning and incomplete Si burning in the Population III supernova/hypernova, in contrast to the suggestion that Ca is originated from the hot-CNO cycle during pre-supernova evolution. Chemical abundances of four carbon-rich iron-poor stars with $[\text{Fe}/\text{H}] < -4.5$, including SMSS J031300.36–670839.3, are consistently explained by faint supernova models with ejected masses of ^{56}Ni less than $10^{-3} M_{\odot}$.

Key words: stars: abundances – stars: Population III – supernovae: general

Online-only material: color figures

1. INTRODUCTION

Characteristic masses of the first stars (Population III or Pop III stars) and the nature of their supernova explosions are critically important in determining their role in the cosmic reionization and subsequent star formation in the early universe (e.g., Bromm & Yoshida 2011). Cosmological simulations have shown that Pop III stars could be very massive $\gtrsim 100 M_{\odot}$ as a result of cooling of primordial gas via hydrogen molecules (e.g., Bromm & Larson 2004). More recent studies, however, propose mechanisms in which lower-mass stars can form through radiation feedback from growing protostars and/or disk fragmentation (Hosokawa et al. 2011; Clark et al. 2011; Hirano & Yoshida 2013; Bromm 2013; Susa 2013).

Abundance patterns of the lowest-metallicity stars in our Galaxy provide us with a rare opportunity to observationally constrain the masses of Pop III stars. The chemical abundances in the four iron-poor stars with $[\text{Fe}/\text{H}] < -4.5$, HE 0107–5240 (Christlieb et al. 2002, 2004), HE 1327–2326 (Frebel et al. 2005; Aoki et al. 2006), HE 0557–4840 (Norris et al. 2007), and SDSS J102915+172927 (Caffau et al. 2011; see Hansen et al. 2014 for a recent discovery of another metal-poor star in this metallicity range), do not show signatures of pair-instability supernovae of very massive ($\gtrsim 140 M_{\odot}$) stars as their progenitors (Nomoto et al. 2013, and references therein). Instead, the observed abundances in these stars are better explained by the yields of core-collapse supernovae of moderately massive Pop III stars with several tens of M_{\odot} (Umeda & Nomoto 2002, 2003; Limongi et al. 2003; Iwamoto et al. 2005; Tominaga 2009; Tominaga et al. 2007b, 2014; Heger & Woosley 2010; Kobayashi et al. 2014).

Another important insight into the nature of the Pop III stars is that a large fraction of most iron-poor stars are carbon-rich (e.g., Hansen et al. 2014). Iwamoto et al. (2005) suggest that the large

enhancement of carbon observed in both HE 0107–5240 and HE 1327–2326 is explained by their models with the mixing of supernova ejecta and their subsequent fallback on to the central remnant. These models, with different extents of mixing regions, simultaneously reproduce the observed similarity in $[\text{C}/\text{Fe}]$ and more than a factor of ~ 10 differences in $[\text{O}, \text{Mg}, \text{Al}/\text{Fe}]$ between the two stars.

A metal-poor star, SMSS J031300.36–670839.3 (SMSS J0313–6708), recently discovered by the SkyMapper Southern Sky Survey, provides us with a new opportunity to test theoretical predictions about Pop III stars (Keller et al. 2007, 2014). Follow-up spectroscopic observations found that this object shows an extremely low upper limit for its iron abundance ($[\text{Fe}/\text{H}] < -7.1$), more than 1.0 dex lower than the previous record of the lowest iron-abundance stars.

In this Letter, we extend the study of Iwamoto et al. (2005) and examine whether the abundances of the five stars with $[\text{Fe}/\text{H}] < -4.5$, including the most iron-deficient star SMSS 0313–6708, can be consistently explained by the supernova yields of Pop III stars that undergo mixing and fallback.

2. MODELS

We employ the Pop III supernova/hypernova yields of progenitors with main-sequence masses of $M = 25 M_{\odot}$ (Iwamoto et al. 2005) and $40 M_{\odot}$ (Tominaga et al. 2007a) and assume kinetic explosion energies, E , of $E_{51} = E/10^{51}$ erg = 1, 10 for the $25 M_{\odot}$ model and $E_{51} = 1, 30$ for the $40 M_{\odot}$ model in the same way as in Tominaga et al. (2007b). The abundance distribution after explosions of the $25 M_{\odot}$ models with $E_{51} = 1$ and 10 as a function of the enclosed mass (M_r) is illustrated in Figure 1.

For the parameters that describe the extent of the mixing fallback, we follow the prescription of Umeda & Nomoto (2002) and Tominaga et al. (2007b) as briefly summarized below. We assume that the supernova ejecta within an M_r range between an initial mass cut $M_{\text{cut}}(\text{ini})$ and $M_{\text{mix}}(\text{out})$ are mixed, and a

⁴ Hamamatsu Professor.

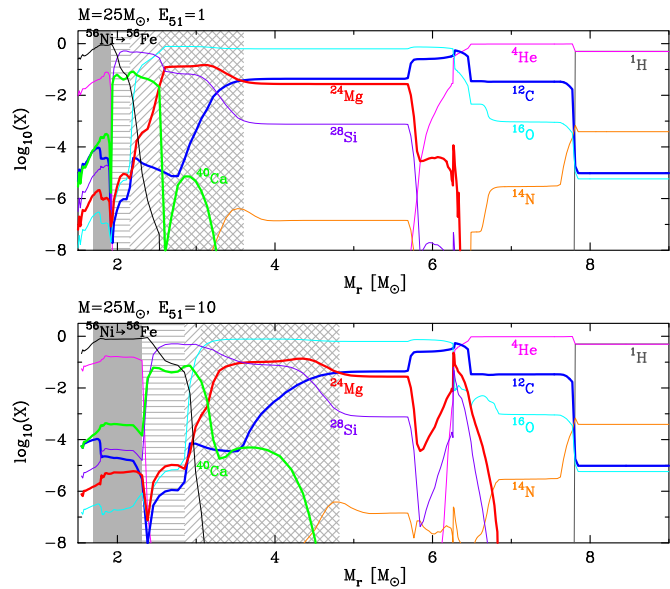


Figure 1. Top: the distribution of elemental abundances as a function of the enclosed mass (M_r) for a model with $M = 25 M_\odot$ and $E_{51} = 1$. Regions where explosive burning takes place are shown with filled (complete Si burning), bordered (incomplete Si burning), hatched (O burning), and cross-hatched (C burning) areas. Bottom: same as the top panel but for a model with $M = 25 M_\odot$ and $E_{51} = 10$.

(A color version of this figure is available in the online journal.)

fraction f of the mixed material falls back onto the central remnant, presumably forming a black hole. This approach has been compared with a hydrodynamical calculation of jet-induced explosions (Tominaga 2009) and it is demonstrated that the prescription of the mixing fallback applied to a one-dimensional calculation mimics an angle-averaged yield of aspherical supernovae.

We assume that the $M_{\text{cut}}(\text{ini})$ is approximately located at the outer edge of the Fe core ($M_r = 1.79 M_\odot$ and $2.24 M_\odot$ for $M = 25 M_\odot$ and $40 M_\odot$, respectively; Tominaga et al. 2007b). The value of $M_{\text{cut}}(\text{ini})$ is varied within $\pm 0.3 M_\odot$ with steps of $0.1 M_\odot$ to better fit the observed abundance patterns. Then, we calculate the grids of supernova yields for the range of $\log f = -7.0$ – 0.0 with steps of $\Delta \log f = 0.1$ and for $M_{\text{mix}}(\text{out}) = 1.5$ – $9.0 M_\odot$ ($M = 25 M_\odot$) and 2.0 – $16.0 M_\odot$ ($M = 40 M_\odot$) with steps of $\Delta M_{\text{mix}}(\text{out}) = 0.1 M_\odot$. These ranges have been chosen so that the $M_{\text{mix}}(\text{out})$ is searched approximately in the range between the location of the $M_{\text{cut}}(\text{ini})$ and the outer boundary of the CO core (see Figure 1). Using this grid of yields, parameter sets ($M_{\text{cut}}(\text{ini})$, $M_{\text{mix}}(\text{out})$, f) that reproduce the observed [C/Ca] and [C/Mg] ratios in SMSS 0313–6708 are searched. In addition to SMSS 0313–6708, we adopt the same parameter-search method for the four other iron-poor stars with [Fe/H] < -4.5 (see Tominaga et al. 2014 for models with other E).

We adopt the observational data analyzed with three-dimensional (3D) and/or NLTE corrections (see the captions of Figures 2 and 3 for details) and normalized with the solar abundances of Asplund et al. (2009). For Ca abundances, we use abundances estimated from Ca I lines for the four other iron-poor stars. We should note, however, that there are uncertainties in the Ca abundances for the 3D and NLTE effects (e.g., Korn et al. 2009; Lind et al. 2013), which affects the normalization of Figure 3. We also consider Ca II abundances when we draw our conclusions.

3. RESULT

Table 1 summarizes the model parameters ($M_{\text{cut}}(\text{ini})$, $M_{\text{mix}}(\text{out})$, f) that best reproduce the observed abundance patterns of the five iron-poor stars. The resultant masses of the central remnant (M_{rem}) and ejected masses of ^{56}Ni , which finally decays to ^{56}Fe , are indicated in the last two columns. Since only C, Mg, and Ca have been measured for SMSS 0313–6708, all four models ($(M, E_{51}) = (25, 1)$, $(25, 10)$, $(40, 1)$, and $(40, 30)$) can equally well fit the observed abundance ratios as indicated in Table 1. For the other four stars, the parameters have been constrained using a larger number of elements and thus only the best-fit models are shown.

3.1. The Best-fit Models for SMSS 0313–6708

Figure 2 shows the abundance patterns relative to Ca of the best-fit models for $M = 25 M_\odot$ (top) and $40 M_\odot$ (bottom). In each panel, the models of the supernova ($E_{51} = 1$; solid lines with squares) and hypernovae ($E_{51} = 10$ and 30 for $M = 25 M_\odot$ and $40 M_\odot$; solid lines with triangles) are shown with the observed abundances in SMSS 0313–6708 (filled circles and arrows for the upper limits). In the following, we describe the comparison of each model with the observed abundance pattern.

$M = 25 M_\odot$, $E_{51} = 1$, *supernova model*. The model yield that fits the observed [C/Ca] and [Mg/Ca] ratios is consistent with the upper limits of other elements except for Na and Al. Because the predicted Na and Al abundances vary by more than a few dex depending on overshooting (Iwamoto et al. 2005) and stellar rotation (Meynet et al. 2010), and on the reaction rate of $^{12}\text{C}(\alpha, \gamma)^{16}\text{O}$ (Chieffi & Limongi 2002, and references therein) in the pre-supernova models, we restrict our discussion for Na and Al to their relative yields between the supernova and hypernova models.

In our model, the observed large [Mg/Ca] ratio results from the large mixing region ($M_{\text{mix}}(\text{out}) = 5.6 M_\odot$) and the small ejected fraction, f , as seen in Figure 1, the material in the layer containing Ca mostly falls back while the material in the outer layer containing Mg is partly ejected. The abundances of iron-peak elements in the model depend on the adopted $M_{\text{cut}}(\text{ini})$. For $M_{\text{cut}}(\text{ini}) = 2.0 M_\odot$, the ejected mass of ^{56}Ni is less than $10^{-5} M_\odot$ for these models, which is extremely small compared to those estimated for nearby supernovae ($^{56}\text{Ni} \sim 0.1 M_\odot$; Blinnikov et al. 2000; Nomoto et al. 2013).

$M = 25 M_\odot$, $E_{51} = 10$, *hypernova model*. The higher explosion energy induces explosive burning at the bottom of the He layer, which leads to extra production of Mg at $M_r \sim 6 M_\odot$, as can be seen in the bottom panel of Figure 1. Consequently, a large value of $M_{\text{mix}}(\text{out})$ ($6.4 M_\odot$), which results in a large fallback of Mg synthesized at $M_r \sim 6 M_\odot$, best explains the observed [C/Mg] ratio. The [O/Ca] ratio is smaller than that of the supernova model as a result of the associated fallback of oxygen for the given [Mg/Ca] ratio. The [O/Ca] ratio, however, can be as large as $\sim +4$ depending on $M_{\text{mix}}(\text{out})$ and f , as shown by the dotted gray line in Figure 2.

The [Na/Ca] and [Al/Ca] ratios of the hypernova yields are lower than those predicted by the supernova model. This is due to the more extended explosive O- and C-burning regions in the more energetic explosion (cross-hatched regions in Figure 1, in which more Na and Al are consumed to synthesize heavier nuclei; Nakamura et al. 2001). The larger $M_{\text{mix}}(\text{out})$ with small f also leads to the smaller amount of ejected Na and Al than the supernova model.

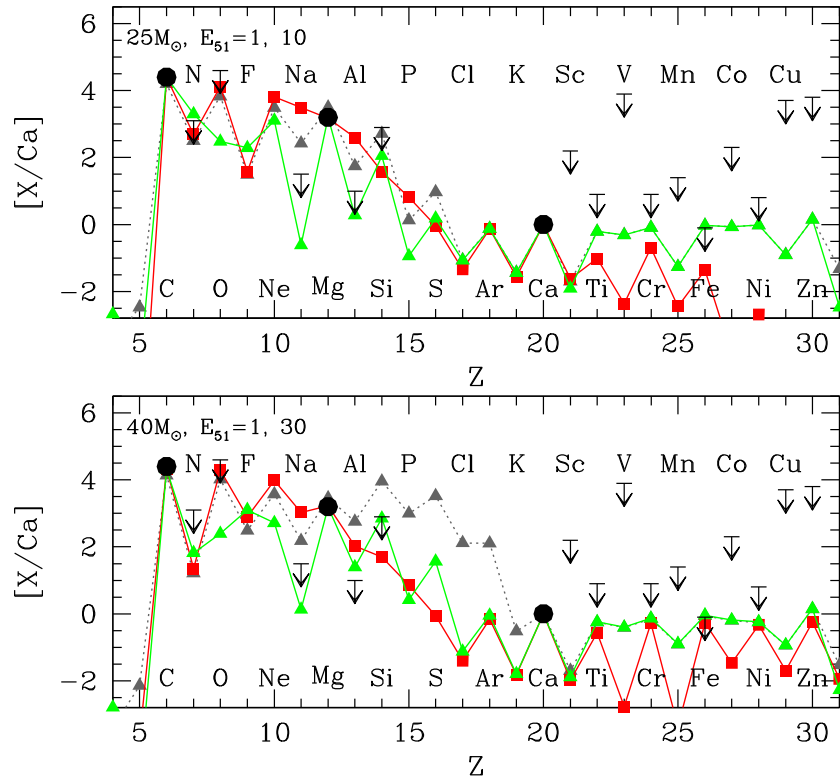


Figure 2. Elemental abundance patterns (relative to Ca) of the best-fit models for SMSS 0313–6708 (observational data from Keller et al. 2014 with 3D–NLTE; filled circles and arrows for the upper limits) for $M = 25 M_{\odot}$ (top) and $40 M_{\odot}$ (bottom). The solid lines with squares (red) show the supernova model with $E_{51} = 1$. The solid lines with triangles (green) show the hypernova model with $E_{51} = 10$ (for $M = 25 M_{\odot}$) and $E_{51} = 30$ ($40 M_{\odot}$). The dotted lines with triangles (gray) indicate another hypernova model with different parameters from the best-fit model ($M_{\text{mix}}(\text{out}) = 5.7 M_{\odot}$ and $\log f = -5$).

(A color version of this figure is available in the online journal.)

Table 1
Summary of the Observed Abundances and the Best-fit Models

Name	[Fe/H] ^a (dex)	[C/Ca] ^a (dex)	[C/Mg] ^a (dex)	M (M_{\odot})	E_{51} (10^{51} erg)	$M_{\text{cut}}(\text{ini})$ (M_{\odot})	$M_{\text{mix}}(\text{out})$ (M_{\odot})	$\log f$	M_{rem} (M_{\odot})	$M(^{56}\text{Ni})$ (M_{\odot})
SMSSJ0313–6708	<−7.1	4.4	1.2	25	1	2.0	5.6	−5.1	5.6	2.1×10^{-7}
				25	10	1.7	6.4	−5.8	6.4	1.1×10^{-6}
				40	1	2.0	12.7	−5.4	12.7	3.4×10^{-6}
				40	30	2.5	14.3	−6.0	14.3	1.9×10^{-6}
HE0107–5240	−5.7	2.9	2.6	25	1	1.7	5.7	−3.3	5.7	1.4×10^{-4}
HE1327–2326	−6.0	3.3	1.8	25	1	1.7	5.7	−4.4	5.7	1.1×10^{-5}
HE0557–4840	−4.9	1.2	1.1	25	1	1.7	5.7	−2.1	5.7	2.2×10^{-3}
SDSSJ102915+172927	−4.9	<0.1	<0.1	40	30	2.0	5.5	−0.9	6.0	2.8×10^{-1}

Note. ^a See the captions of Figures 2 and 3 for references of the observational data.

The abundance differences between the odd and even atomic number iron-peak elements are smaller for the hypernova model. This results from enhanced production of odd- Z iron-peak elements due to the higher entropy and larger neutron excess in the Si-burning region in the more energetic explosion (e.g., Nakamura et al. 2001).

$M = 40 M_{\odot}$, $E_{51} = 1$, *supernova model*. Compared to the supernova model with $M = 25 M_{\odot}$, the outer boundary of the Mg-rich layer extends to a larger mass at $M_r \sim 13 M_{\odot}$. Consequently, the models with $M_{\text{mix}}(\text{out}) \sim 12\text{--}14 M_{\odot}$ best fit the observed [C/Mg] ratio.

$M = 40 M_{\odot}$, $E_{51} = 30$, *hypernova model*. The hypernova model for the $40 M_{\odot}$ progenitor is characterized by larger [Si/Ca] and [S/Ca] ratios because of a more extended explosive O- and C-burning region, in which elements such as O and C are consumed to synthesize Si and S. Aluminum is also synthesized in the explosive C-burning layer but destroyed in the explosive

O-burning layer to synthesize Si. In comparison to the supernova model, predicted abundances of V, Mn, Co, and Cu relative to Ca are larger, similar to the $25 M_{\odot}$ hypernova model.

3.2. Four Other Iron-poor Stars with $[\text{Fe}/\text{H}] < -4.5$

Figure 3 shows the abundance patterns of the best-fit models for four other iron-poor stars with $[\text{Fe}/\text{H}] < -4.5$. We note that the N abundances are not included from the fitting because of their uncertainty in the progenitor models (Iwamoto et al. 2005). For the three carbon-enhanced stars (HE 1327–2326, HE 0107–5240, and HE 0557–4840) shown in the top three panels, the supernova models of $M = 25 M_{\odot}$ with $E_{51} = 1$ adopting the parameters $M_{\text{mix}}(\text{out}) \sim 5.7 M_{\odot}$ and $f \sim 10^{-4}\text{--}10^{-2}$ best explain the observed abundances (squares). The hypernova models with $E_{51} = 10$ (triangles) tend to yield higher [Mg/Ca]

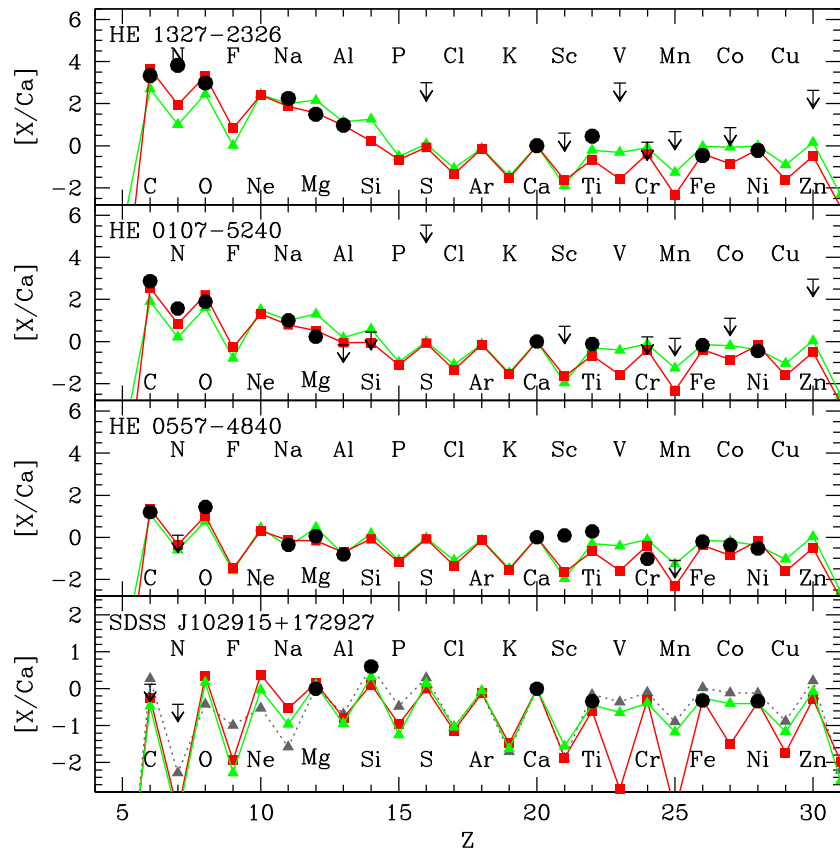


Figure 3. Elemental abundance patterns (relative to Ca derived from Ca I lines) of the best-fit models for the four other iron-poor stars with $[\text{Fe}/\text{H}] < -4.5$. The squares (red) and triangles (green) show supernova and hypernova models, respectively, with $M = 25 M_{\odot}$ ($E_{51} = 1$ or 10) for the three carbon-enhanced stars (top three panels) and $M = 40 M_{\odot}$ ($E_{51} = 1$ or 30) for the star without carbon enhancement (bottom panel). The gray triangles with a dotted line in the bottom panel indicate the hypernova model with an alternative set of parameters ($M_{\text{mix}}(\text{out}) = 13.9$, $\log f = -1.9$). Observational data sources are HE 0107–5240: Collet et al. (2006) with 3D-LTE; HE 1327–2326: Frebel et al. (2008) with 3D-LTE and Bonifacio et al. (2012) for S with 3D-NLTE; HE 0557–4840: Norris et al. (2007, 2012) with 3D-LTE; and SDSS J102915 + 172927: Caffau et al. (2012) with 3D-NLTE.

(A color version of this figure is available in the online journal.)

ratios than the observed values, which is due to the explosive synthesis of Mg at the bottom of the He layer.

The abundance pattern of SDSS J102915 + 172927 with no carbon enhancement is in better agreement with the hypernova yields of $M = 40 M_{\odot}$ and $E_{51} = 30$ (triangles). This is due to the relatively high $[\text{Si}/\text{Ca}]$ ratio observed in this star, which is better explained by the larger Si/Ca ratio in the higher explosion energy model. Such an energy dependence can be understood from the comparison of the abundance distributions between the top and bottom panels of Figure 1. In the hypernova model (bottom), the region where the post-shock temperature becomes high enough to produce a significant amount of Si extends to larger M_r than in the supernova model (top).

3.3. Comparison of the Five Most Iron-poor Stars

Figure 4 summarizes the best-fit parameters ($M_{\text{mix}}(\text{out})$, $\log f$) obtained for the five iron-poor stars (star: SMSS 0313–6708, square; HE 1327–2326, pentagon; HE 0107–5240, three-pointed star; HE 0557–4840, and asterisk; SDSS J102915 + 172927). The results for the model $(M, E_{51}) = (25, 1)$, $(25, 10)$, $(40, 1)$, and $(40, 30)$ are shown from the top-left to bottom-right panels. The regions where the $[\text{C}/\text{Ca}]$ and $[\text{C}/\text{Mg}]$ ratios measured within $\pm 3\sigma$ in SMSS 0313–6708 are realized are shown in orange and green, respectively.

In the $M_{\text{mix}}(\text{out})$ – $\log f$ parameter space, the $[\text{C}/\text{Ca}]$ ratio is at maximum when $M_{\text{mix}}(\text{out})$ is located at the layer where carbon

burning takes place ($M_r \sim 3$ – $4 M_{\odot}$ in the $M = 25 M_{\odot}$ and $E_{51} = 1$ model; top panel of Figure 1). At a given $M_{\text{mix}}(\text{out})$, the $[\text{C}/\text{Ca}]$ is larger for smaller f (larger fallback), because Ca synthesized in the inner layer falls back more efficiently for smaller f than C synthesized in the outer layer. As a result, the high $[\text{C}/\text{Ca}]$ ratio (orange in Figure 4) in SMSS 0313–6708 is reproduced with an extensive fallback ($\log f < -4$).

The $[\text{C}/\text{Mg}]$ ratio is at maximum when the $M_{\text{mix}}(\text{out})$ is located at the outer edge of the Mg-rich ejecta. The ejection of a large amount of C and the fallback of most of the Mg-rich layer lead to the large $[\text{C}/\text{Mg}]$ ratios. The observed $[\text{C}/\text{Mg}]$ ratio in SMSS 0313–6708 is close to the maximum for the observed $[\text{C}/\text{Ca}]$. Consequently, mixing up to $M_r \sim 6 M_{\odot}$ (for $M = 25 M_{\odot}$) and $\sim 13 M_{\odot}$ (for $M = 40 M_{\odot}$) and small f are required (green in Figure 4). We note that the gap in the $[\text{C}/\text{Mg}]$ constraint, which is only seen in the hypernova models, stems from the explosive Mg production in the energetic explosion (Section 3.1). The resultant $[\text{C}/\text{Mg}]$ ratio at the gap is lower than the observed $[\text{C}/\text{Mg}]$ ratio.

For the three other iron-poor stars showing carbon enhancement, the best-fit value of $M_{\text{mix}}(\text{out})$ is as large as that required for SMSS 0313–6707 with $\log f \leq -2$. The obtained parameters $M_{\text{mix}}(\text{out})$ and f remain similar if we take the average of Ca I and Ca II abundances instead of Ca I abundances, which gives 0.2 dex systematically lower $[\text{C}/\text{Ca}]$ than in Table 1. They also remain similar if only C, Mg, and Ca abundances are taken into account in the fitting. This is because these elements are syn-

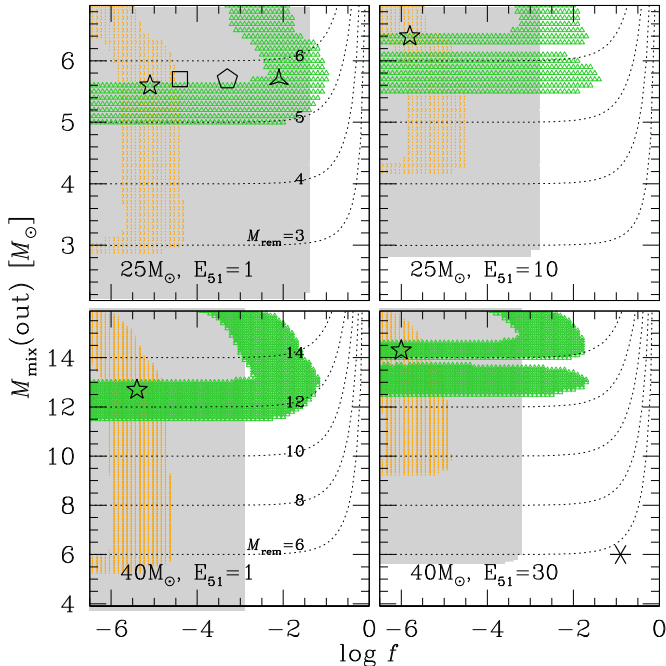


Figure 4. Regions in the $M_{\text{mix}}(\text{out})$ – $\log f$ parameter space for the observed $[\text{C}/\text{Ca}]$ (orange) and $[\text{C}/\text{Mg}]$ (green) ratios within $\pm 3\sigma$ errors. The best-fit parameters for SMSS 0313–6708 in each model are shown with stars. The best-fit models for HE 1327–2326 (square), HE 0107–5240 (pentagon), HE 0557–4840 (three-pointed star), and SDSS J102915 + 172927 (asterisk) are also shown. The dotted lines indicate the remnant mass in the corresponding parameter set. The region that represents a relatively faint supernova with $M(^{56}\text{Ni}) < 10^{-3} M_{\odot}$ is shown in gray.

(A color version of this figure is available in the online journal.)

thesized in the different layers and are dominant in each layer (the thick lines in Figure 1), and thus their abundance ratios are mostly determined by the mixing fallback.

The abundance pattern of SDSS J102915 + 172927, which does not show carbon enhancement, is best reproduced by the $40 M_{\odot}$ model with $M_{\text{mix}}(\text{out}) = 6.0 M_{\odot}$ and $\log f = -0.9$ (asterisk in Figure 4). If we use the average of Ca I and Ca II abundances, a model with $M_{\text{mix}}(\text{out}) = 13.9 M_{\odot}$ and $\log f = -1.9$ best reproduces the observed abundances (gray triangles with the dotted line in the bottom panel of Figure 3).

The differences in masses, energies, and the state of mixing fallback in the fitted models may explain populations with and without carbon enhancement in the Galactic halo stars (e.g., Norris et al. 2013). Analyses based on a larger number of samples are required to examine whether or not the properties of Pop III supernovae/hypernovae can reproduce the abundance patterns and the relative fraction of the C-enhanced and the C-normal metal-poor populations in the Galactic halo.

The gray-filled region in Figure 4 represents the range of parameters that give the ejected Fe mass less than $10^{-3} M_{\odot}$, which presumably corresponds to faint Pop III supernovae. All three stars showing the C enhancement are located in the faint supernova region.

4. DISCUSSION

As shown in the previous section, the abundance measurements (C, Mg, and Ca) in SMSS 0313–6707 are reproduced with Pop III supernova/hypernova yields ($(M, E_{51}) = (25, 1), (25, 10), (40, 1), \text{ and } (40, 30)$), with the model

parameters corresponding to faint supernovae/hypernovae with extensive mixing and prominent fallback. In order to discriminate between models with different masses and energies, additional abundance measurements for oxygen as well as iron-peak elements including V, Mn, Co, and Cu are particularly useful.

The ejected mass of ^{40}Ca is only $\sim 10^{-7}$ – $10^{-8} M_{\odot}$ in the faint supernova/hypernova models. To be compatible with the observed calcium abundance ($[\text{Ca}/\text{H}] = -7.0$), the supernova ejecta should be diluted with $\sim 10^3$ – $10^4 M_{\odot}$ of the primordial gas. In the case of supernova models with $E_{51} = 1$, this is consistent with the suggested relation between the supernova energy versus the swept-up gas mass with primordial composition (Thornton et al. 1998), as adopted in Tominaga et al. (2007b), for the assumed number density of hydrogen $1 < n_{\text{H}} < 100 \text{ cm}^{-3}$. On the other hand, this relation predicts that the hypernova sweeps up a much larger amount of hydrogen ($\gtrsim 10^5 M_{\odot}$ for $n_{\text{H}} < 10^4 \text{ cm}^{-3}$) than the above values. Recent cosmological simulations of the transport of metals synthesized in a Pop III supernova, however, suggest a wide range of metal abundances in the interstellar gas clouds after the explosion of a Pop III star (Ritter et al. 2012), and thus the hypernova could work as a source of chemical enrichment for the formation of stars with $[\text{Ca}/\text{H}] \lesssim -7$.

In our model, Ca is produced by hydrostatic/explosive O burning and incomplete Si burning in Pop III supernovae or hypernovae with masses of 25 or $40 M_{\odot}$. This is different from the $60 M_{\odot}$ model adopted in Keller et al. (2014), where Ca is originated from the hot-CNO cycle during the main-sequence phase. Synthesis of $\sim 10^{-7} M_{\odot}$ Ca in the hot-CNO cycle is also seen in the $100 M_{\odot}$ models of Umeda & Nomoto (2005). On the other hand, Ca produced in this mechanism is not seen in the 25 and $40 M_{\odot}$ progenitors analyzed in this Letter. The mass fraction of Ca near the bottom of the hydrogen layer in these progenitors is $\log X_{\text{Ca}} < -10$.

In order to clarify which of these nucleosynthesis sites are responsible for the observed Ca, we note a different prediction between the two scenarios. Our models suggest that a certain amount of Fe distributed in the inner region as well as explosively synthesized Ca are ejected as a result of the assumed mixing at $M_r = 2$ – $6 M_{\odot}$. This results in an $[\text{Fe}/\text{Ca}]$ ratio of ~ -2 – 0 , depending on the $M_{\text{cut}}(\text{ini})$. Consequently, our models of the faint supernova/hypernova predict the metallicity distribution function (MDF) to be continuous even below $[\text{Fe}/\text{H}] < -6$. On the other hand, the model adopted in Keller et al. (2014), in which Ca is produced in the hot-CNO cycle, predicts $[\text{Fe}/\text{Ca}] \lesssim -3$, which is not observed in other extremely iron-poor stars. Because of the distinct Ca production sites, the MDF could be discontinuous in the most metal-poor region. Future photometric and spectroscopic surveys to discover the lowest-metallicity stars and their MDF will provide clues to discriminate these mechanisms.

The models adopted in this work suggest that faint Pop III supernovae could be the origin of the observed abundance patterns and the variation among the most iron-poor carbon-rich stars. To understand the physics of faint Pop III supernovae, multi-dimensional simulations are necessary. Large-scale mixing, as suggested for carbon-enhanced stars, is not predicted in the models with Rayleigh–Taylor mixing alone (Joggerst et al. 2009). Instead, a more likely origin of such large-scale mixing fallback would be the jet-induced supernovae/hypernovae, where the inner material can be ejected along the jet axis, while a large fraction of the material along the equatorial plane falls back (Tominaga 2009).

This work has been supported by the Grant-in-Aid for JSPS fellow (M.N.I.) and for Scientific Research of the JSPS (23224004, 23540262, 26400222), and by the WPI Initiative, MEXT, Japan. The authors thank S. Keller, M. Asplund, and K. Lind for fruitful discussions. We are also grateful to the referees for their valuable comments and suggestions which helped improve this paper.

REFERENCES

- Aoki, W., Frebel, A., Christlieb, N., et al. 2006, *ApJ*, 639, 897
- Asplund, M., Grevesse, N., Sauval, A. J., & Scott, P. 2009, *ARA&A*, 47, 481
- Blinnikov, S., Lundqvist, P., Bartunov, O., et al. 2000, *ApJ*, 532, 1132
- Bonifacio, P., Caffau, E., Venn, K. A., & Lambert, D. L. 2012, *A&A*, 544, 102
- Bromm, V. 2013, *RPPH*, 76, 2901
- Bromm, V., & Larson, R. B. 2004, *ARA&A*, 42, 79
- Bromm, V., & Yoshida, N. 2011, *ARA&A*, 49, 373
- Caffau, E., Bonifacio, P., François, P., et al. 2011, *Natur*, 477, 67
- Caffau, E., Bonifacio, P., François, P., et al. 2012, *A&A*, 542, 51
- Chieffi, A., & Limongi, M. 2002, *ApJ*, 577, 281
- Christlieb, N., Bessell, M. S., Beers, T. C., et al. 2002, *Natur*, 419, 904
- Christlieb, N., Gustafsson, B., Korn, A., et al. 2004, *ApJ*, 603, 708
- Clark, P. C., Glover, S. C. O., Klessen, R. S., & Bromm, V. 2011, *ApJ*, 727, 110
- Collet, R., Asplund, M., & Trampedach, R. 2006, *ApJL*, 644, L121
- Frebel, A., Aoki, W., Christlieb, N., et al. 2005, *Natur*, 434, 871
- Frebel, A., Collet, R., Eriksson, K., Christlieb, N., & Aoki, W. 2008, *ApJ*, 684, 588
- Hansen, T., Hansen, C. J., Christlieb, N., et al. 2014, *ApJ*, 787, 162
- Heger, A., & Woosley, S. E. 2010, *ApJ*, 724, 341
- Hirano, S., & Yoshida, N. 2013, *ApJ*, 763, 52
- Hosokawa, T., Omukai, K., Yoshida, N., & Yorke, H. W. 2011, *Sci*, 334, 1250
- Iwamoto, N., Umeda, H., Tominaga, N., Nomoto, K., & Maeda, K. 2005, *Sci*, 309, 451
- Joggerst, C. C., Woosley, S. E., & Heger, A. 2009, *ApJ*, 693, 1780
- Keller, S. C., Bessel, M. S., Frebel, A., et al. 2014, *Natur*, 506, 463
- Keller, S. C., Schmidt, B. P., Bessel, M. S., et al. 2007, *PASA*, 25, 1
- Kobayashi, C., Ishigaki, N. M., Tominaga, N., & Nomoto, K. 2014, *ApJL*, 785, L5
- Korn, A. J., Richard, O., Mashonkina, L., et al. 2009, *ApJ*, 698, 410
- Limongi, M., Chieffi, A., & Bonifacio, P. 2003, *ApJL*, 594, L123
- Lind, K., Melendez, J., Asplund, M., Collet, R., & Magic, Z. 2013, *A&A*, 554, 96
- Meynet, G., Hirschi, R., Ekstrom, S., et al. 2010, *A&A*, 521, 30
- Nakamura, T., Umeda, H., Iwamoto, K., et al. 2001, *ApJ*, 555, 880
- Nomoto, K., Kobayashi, C., & Tominaga, N. 2013, *ARA&A*, 51, 457
- Norris, J. E., Christlieb, N., Bessell, M. S., et al. 2012, *ApJ*, 753, 150
- Norris, J. E., Christlieb, N., Korn, A. J., et al. 2007, *ApJ*, 670, 774
- Norris, J. E., Yong, D., Bessell, M. S., et al. 2013, *ApJ*, 762, 28
- Ritter, J. S., Safrank-Shrader, C., Gnat, O., Milosavljević, M., & Bromm, V. 2012, *ApJ*, 761, 56
- Susa, H. 2013, *ApJ*, 773, 185
- Thornton, K., Gaudlitz, M., Janka, H.-Th., & Steinmetz, M. 1998, *ApJ*, 500, 95
- Tominaga, N. 2009, *ApJ*, 690, 526
- Tominaga, N., Iwamoto, N., & Nomoto, K. 2014, *ApJ*, 785, 98
- Tominaga, N., Maeda, K., Umeda, H., et al. 2007a, *ApJL*, 657, L77
- Tominaga, N., Umeda, H., & Nomoto, K. 2007b, *ApJ*, 660, 516
- Umeda, H., & Nomoto, K. 2002, *ApJ*, 565, 385
- Umeda, H., & Nomoto, K. 2003, *Natur*, 422, 871
- Umeda, H., & Nomoto, K. 2005, *ApJ*, 619, 427